Agricultural and Forest Meteorology 247 (2017) 280–292

Contents lists available at ScienceDirect

Agricultural and Forest Meteorology

journal homepage: www.elsevier.com/locate/agrformet

On the relationship between continuous measures of canopy greenness derived using near-surface remote sensing and satellite-derived vegetation products

Luke A. Brown[a,*], Jadunandan Dash[a], Booker O. Ogutu[a], Andrew D. Richardson[b,c,d]

[a] Geography and Environment, University of Southampton, Highfield, Southampton, SO17 1BJ, United Kingdom
[b] Department of Organismic and Evolutionary Biology, Harvard University, Cambridge, MA 02138, United States
[c] School of Informatics, Computing and Cyber Systems, Northern Arizona University, Flagstaff, AZ 8601, United States
[d] Center for Ecosystem Science and Society, Northern Arizona University, Flagstaff, AZ 86011, United States

ARTICLE INFO

Keywords:
Chlorophyll
FAPAR
MERIS
NDVI
PhenoCam
Validation

ABSTRACT

Over the last two decades, satellite-derived estimates of biophysical variables have been increasingly used in operational services, requiring quantification of their accuracy and uncertainty. Evaluating satellite-derived vegetation products is challenging due to their moderate spatial resolution, the heterogeneity of the terrestrial landscape, and difficulties in adequately characterising spatial and temporal vegetation dynamics. In recent years, near-surface remote sensing has emerged as a potential source of data against which satellite-derived vegetation products can be evaluated. Several studies have focussed on the evaluation of satellite-derived phenological transition dates, however in most cases the shape and magnitude of the underlying time-series are neglected. In this paper, we investigated the relationship between the green chromatic coordinate (GCC) derived using near-surface remote sensing and a range of vegetation products derived from the Medium Resolution Imaging Spectrometer (MERIS) throughout the growing season. Moderate to strong relationships between the GCC and vegetation products derived from MERIS were observed at deciduous forest sites. Weak relationships were observed over evergreen forest sites as a result of their subtle seasonality, which is likely masked by atmospheric, bidirectional reflectance distribution function (BRDF), and shadowing effects. Temporal inconsistencies were attributed to the oblique viewing geometry of the digital cameras and differences in the incorporated spectral bands. In addition, the commonly observed summer decline in GCC values was found to be primarily associated with seasonal variations in brown pigment concentration, and to a lesser extent illumination geometry. At deciduous sites, increased sensitivity to initial increases in canopy greenness was demonstrated by the GCC, making it particularly well-suited to identifying the start of season when compared to satellite-derived vegetation products. Nevertheless, in some cases, the relationship between the GCC and vegetation products derived from MERIS was found to saturate asymptotically. This limits the potential of the approach for evaluation of the vegetation products that underlie satellite-derived phenological transition dates, and for the continuous monitoring of vegetation during the growing season, particularly at medium to high biomass study sites.

1. Introduction

Vegetation is a major component of the biosphere, and the amount and dynamics of vegetation influence a range of biogeochemical processes. Systematic estimates of the biophysical variables that describe vegetation condition are therefore required by the numerical models that enhance our understanding of the environment and climate system (Myneni et al., 2002; Sellers et al., 1997). Such understanding is fundamental to the development of successful environmental policy, and plays a critical role in informing effective climate change mitigation strategy. Estimates of biophysical variables are also essential in the monitoring of forest resources, of which a net loss of 13 million ha per year is estimated to have occurred globally between 2000 and 2010 (FAO, 2010). Similarly, these estimates are highly valuable in the management of agricultural practices, a particularly important consideration in the context of an increasing global population (Foley et al., 2011; Godfray et al., 2010). As a result, parameters such as the fraction of absorbed photosynthetically active radiation (FAPAR) and leaf area

* Corresponding author.
E-mail address: l.a.brown@soton.ac.uk (L.A. Brown).

http://dx.doi.org/10.1016/j.agrformet.2017.08.012
Received 27 January 2017; Received in revised form 9 August 2017; Accepted 10 August 2017
Available online 23 August 2017

index (LAI) have been designated essential climate variables (ECVs) (GCOS, 2012).

The consistent monitoring of vegetation at regional to global scales was first facilitated by the Advanced Very High Resolution Radiometer (AVHRR), which records coarse spectral resolution data at red and near-infrared wavelengths. Over the last two decades, instruments such as the Moderate Resolution Imaging Spectroradiometer (MODIS), Medium Resolution Imaging Spectrometer (MERIS) and Vegetation (VGT) have provided improvements in radiometric, spectral and spatial resolution (Barnes et al., 1998; Maisongrande et al., 2004; Rast et al., 1999). From these data, a range of satellite-derived vegetation products have emerged, providing users with spatially explicit estimates of various biophysical variables. Examples include the CYCLOPES and MOD15 products, which provide estimates of FAPAR and LAI derived from VGT and MODIS respectively (Baret et al., 2007; Knyazikhin et al., 1999; Myneni et al., 1999), in addition to the MERIS Global Vegetation Index (MGVI), which corresponds to FAPAR (Gobron et al., 1999), and the MERIS Terrestrial Chlorophyll Index (MTCI), a surrogate of canopy chlorophyll content (Dash and Curran, 2004). Over the coming years, the continuity of these products will be ensured by new instruments such as the Ocean and Land Colour Instrument (OLCI), Sea and Land Surface Temperature Radiometer (SLSTR), and Visible Infrared Radiometer Suite (VIIRS) (Donlon et al., 2012; Justice et al., 2013).

To be of real use in environmental decision making, it is vital to ensure that satellite-derived vegetation products are of high quality and consistency. This is a particularly important consideration as we enter the era of operational use, in which an increasing number of products will be routinely made available through initiatives such as the European Commission's Copernicus programme (EC, 2005). Scientists, decision makers, and service providers will be provided with an unprecedented volume of data from which to choose, supporting activities such as agricultural monitoring and food security, forest management, numerical weather prediction, and climate modelling. By quantifying the uncertainties associated with satellite-derived vegetation products, their performance can be better understood, enabling users to assess their fitness for purpose and select those data that are most appropriate for their needs (Baret et al., 2005; Justice et al., 2000; Morisette et al., 2002, 2006). The importance of product evaluation is increasingly well recognised, and in recent years initiatives such as the Quality Assurance Framework for Earth Observation (QA4EO) have been established with the endorsement of the Committee on Earth Observation Satellites (CEOS), providing a formal structure for these activities (QA4EO, 2010).

Despite its importance, the evaluation of operational satellite-derived vegetation products is particularly challenging as a result of their moderate spatial resolution, which typically ranges from 300 m to 1 km. The in-situ observations that act as reference data are point-based, making direct comparison possible only in areas of high homogeneity (Fernandes et al., 2014; Morisette et al., 2002). Because such homogeneity is uncommon in the terrestrial landscape, particularly at the spatial resolutions of instruments such as MODIS and MERIS, logistically challenging field campaigns are required to adequately characterise spatial variability over a study site. Unfortunately, these activities are constrained by financial resources, reducing their frequency to, at best, a handful of dates per year, thus limiting the extent to which seasonal vegetation dynamics can be characterised.

In recent years, near-surface remote sensing has emerged as a potential source of data against which satellite-derived vegetation products can be evaluated, providing potentially valuable information about their performance. Digital cameras provide an inexpensive means by which the greenness of a vegetation canopy can be characterised at a high temporal resolution (Keenan et al., 2014; Richardson et al., 2007; 2009; Sonnentag et al., 2012). By making use of the red, green and blue bands of the image, vegetation indices such as the Excess Green Index (EGI) and Green Chromatic Coordinate (GCC) can be calculated, providing a measure of canopy greenness. Importantly, because the field-of-view (FOV) of a digital camera can incorporate an entire canopy, near-surface remote sensing can provide a greater degree of spatial integration than traditional in-situ techniques, better reflecting the moderate spatial resolution of the satellite-derived vegetation products themselves (Hufkens et al., 2012; Keenan et al., 2014; Richardson et al., 2007, 2009).

The phenological research community have adopted near-surface remote sensing as an alternative to traditional in-situ observations of events such as bud-burst and leaf opening, which are limited in terms of their spatial extent and species diversity. By analysing time-series of near-surface remote sensing data, phenological transition dates can be determined (Ide and Oguma, 2010; Richardson et al., 2007, 2009; Sonnentag et al., 2012). Recently, near-surface remote sensing has been used in the continuous monitoring of vegetation condition, and has formed the basis of models of plant function (Hufkens et al., 2016; Migliavacca et al., 2011; Toomey et al., 2015). The Phenological Camera (PhenoCam) network is the largest near-surface remote sensing initiative, and is comprised of 440 sites, each equipped with a digital camera that is mounted above or within a vegetation canopy (Richardson et al., 2007, 2009). Of these 440 sites, 299 adhere to a common protocol, whilst 262 record data at both visible and near-infrared wavelengths. Although the majority of PhenoCam sites are located in North America, similar initiatives have more recently been established in other parts of the world (Morra di Cella et al., 2009; Wingate et al., 2015).

Making use of near-surface remote sensing data provided by initiatives such as the PhenoCam network, several studies have focussed on the evaluation of satellite-derived phenological transition dates (Baumann et al., 2017; Coops et al., 2012; Hufkens et al., 2012; Keenan et al., 2014; Klosterman et al., 2014; Nijland et al., 2016). In these studies, it is only the timing of phenological transition dates that is considered in most cases, whilst the shape and magnitude of the underlying time-series are largely neglected. By focusing on phenological transition dates, rates of change, which can be affected by a range of meteorological and biogeochemical factors, are overlooked. Accurately capturing and representing these dynamics is vital for the continuous monitoring of vegetation condition, and for the modelling of plant function. Recently, several authors have observed features in near-surface remote sensing data that appear unrelated to vegetation dynamics, including a spring peak and summer decline (Keenan et al., 2014; Toomey et al., 2015; Yang et al., 2014). Although previous work has attributed the spring peak to the non-linear relationship between leaf chlorophyll concentration and the GCC (Wingate et al., 2015), the factors responsible for the summer decline remain unclear. If the entire time-series is to be successfully made use of, an increased understanding of these discrepancies is required.

In this paper, we examine the relationship between continuous measures of canopy greenness derived from PhenoCam data and a range of vegetation products derived from MERIS, an instrument with similar characteristics to OLCI on-board the European Space Agency's (ESA's) recently launched Sentinel-3 mission (Donlon et al., 2012; ESA, 2012). In doing so, we hope to answer the following questions:

- How do continuous measures of canopy greenness derived using near-surface remote sensing relate to satellite-derived vegetation products, and what factors are responsible for observed discrepancies?
- Can near-surface remote sensing be used as a means to operationally and systematically evaluate these satellite-derived vegetation products?

2. Materials and methods

2.1. Study sites

14 study sites were selected based on the availability of at least

Table 1
Selected study sites and their characteristics.

Study site	Latitude	Longitude	Elevation (m)	Dominant land cover
Arbutus Lake	43.9821	−74.2332	535	Deciduous forest
Bartlett Experimental Forest (IR)	44.0646	−71.2881	268	Deciduous forest
Cary Institute of Ecosystem Studies	41.7839	−73.7341	127	Deciduous forest
Coweeta Hydrologic Laboratory	35.0596	−83.4280	680	Deciduous forest
Harvard Forest	42.5378	−72.1715	340	Deciduous forest
Harvard Forest Hemlock	42.5394	−72.1780	355	Deciduous forest
Little Prospect Hill	42.5420	−72.1850	380	Deciduous forest
Howland Experimental Forest	45.2041	−68.7403	80	Evergreen forest
Hubbard Brook Experimental Forest	43.9439	−71.7019	253	Deciduous forest
Morgan Monroe State Forest	39.3231	−86.4131	275	Deciduous forest
Proctor Maple Research Center	44.5250	−72.8660	403	Deciduous forest
University of Michigan Biological Station	45.5598	−84.7138	230	Deciduous forest
Vaira Ranch	38.4133	−120.9506	129	Grassland/herbaceous
Wind River Experimental Forest	45.8213	−121.9521	371	Evergreen forest

1 year of near-surface remote sensing data within the time period that MERIS was operational (17/05/2002 to 08/04/2012). Only Type 1 PhenoCam sites were considered, as at these sites a standard installation protocol is adhered to, using a single digital camera model (NetCam SC IR, StarDot Technologies). The study sites meeting these criteria were dominated by deciduous forest, but also incorporated evergreen forest and grassland vegetation. All study sites were located within the United States, lying at a low or moderate elevation (Table 1). With the exception of Vaira Ranch and Wind River, which experience a mediterranean climate, all study sites were characterised by a temperate climate.

2.2. Near-surface remote sensing data

At each study site, near-surface remote sensing data were obtained from the PhenoCam network. Images acquired between the start of PhenoCam operations and the end of the MERIS archive were selected. At the investigated study sites, images are acquired during daylight hours every 30 min. To minimise shadowing and bidirectional reflectance distribution function (BRDF) effects caused by variations in illumination geometry, only near-noon images acquired between the hours of 11:00 and 13:00 local time were considered (Migliavacca et al., 2011; Richardson et al., 2009), providing, on average, 6 images per day. Because the FOV of the digital camera often contained non-canopy features, analysis was restricted to manually defined regions of interest (ROIs) incorporating only the vegetation canopy of interest (Fig. 1). To minimise the effects of atmospheric aerosols and low-lying cloud, ROIs were restricted to the foreground of the image (Richardson, 2009). For each ROI, the GCC was then calculated as

Fig. 1. Example of an ROI incorporating only the vegetation canopy of interest at Coweeta Hydrologic Laboratory (black box).

$$GCC = \frac{DN_{green}}{DN_{red} + DN_{green} + DN_{blue}} \quad (1)$$

where DN_{green}, DN_{red} and DN_{blue} are mean digital number (DN) values in the green, red and blue bands of the image. The GCC is widely used as a measure of canopy greenness, and when compared to alternatives such as the EGI, it is thought to be more effective at supressing the effects of variations in scene illumination (Richardson et al., 2007; Sonnentag et al., 2012). As very few sites were acquiring near-infrared data before the end of the MERIS archive, near-infrared capabilities were not investigated in this study.

Because of the comparatively short atmospheric path associated with near-surface remote sensing data, they are typically subject to minimal atmospheric effects when compared with satellite remote sensing data. Nevertheless, noise may be introduced by external conditions such as rain, fog, and condensation, in addition to variations in scene illumination. To supress such noise, the moving window approach described by Sonnentag et al. (2012) was adopted, in which the 90th percentile of all GCC values acquired within a 3 day window was assigned to the central day. To eliminate residual noise, a simple outlier removal procedure was adopted, in which GCC values lying further than 2 standard deviations from the mean of the time-series were excluded from further analysis.

2.3. Satellite remote sensing data

MERIS level 2 full-resolution full-swath (MER_FRS_2P) data were obtained for a 3 × 3 window (900 m × 900 m) centred on the location of each study site. Over land surfaces, MER_FRS_2P data incorporate two operational vegetation products: the MGVI and MTCI, in addition to bottom-of-atmosphere (BOA) reflectance values in 13 spectral bands. These BOA reflectance values are the result of a partial atmospheric correction for gaseous absorption and Rayleigh scattering (Santer et al., 1999). The 3 × 3 window was selected to minimise uncertainties associated with positional errors and the instrument's point spread function. For each acquisition, the mean value of each measurement data set (MDS) within the window was calculated, except where cloud or relevant product confidence flags were present. These initial data processing steps were carried out remotely using ESA's Grid Processing on Demand (G-POD) environment. By making use of computing resources close to the MERIS archive itself, we could overcome the challenges associated with processing such a large number of acquisitions.

Further data processing was carried out locally using a series of Interactive Data Language (IDL) routines. As a result of known deficiencies in the MERIS cloud-screening algorithm (Gómez-Chova et al., 2007; ESA, 2006), an additional means of quality control was adopted. Because large variations within the 3 × 3 window were only likely under conditions such as partial cloud cover, the coefficient of variation

was calculated, and only acquisitions with a coefficient of varation of <0.50 were retained for further analysis. Such an approach has been previously applied to MERIS data acquired over the marine environment using an arbitrarily determined coefficient of variation of between 0.15 and 0.25 (Barker et al., 2008; Sá et al., 2015; Mélin et al., 2011). As a greater degree of heterogeneity is likely to be experienced over the terrestrial environment, we selected an increased coefficient of variation for the purposes of this study.

Two operational vegetation products were examined: the MGVI and the MTCI. In addition to these products, two alternative vegetation indices were calculated. The Normalised Difference Vegetation Index (NDVI), which demonstrates strong relationships with FAPAR and LAI, was selected as a result of its widespread use (Carlson and Ripley, 1997; Myneni and Williams, 1994; Rouse et al., 1973), whilst the MERIS GCC (hereafter referred to as the MGCC) was selected to provide a more direct spectral comparison to the GCC derived using near-surface remote sensing data. The NDVI was calculated as

$$NDVI = \frac{R_{band\ 13} - R_{band\ 8}}{R_{band\ 13} + R_{band\ 8}} \quad (2)$$

where $R_{band\ 13}$ and $R_{band\ 8}$ are reflectance values in MERIS bands 13 and 8, centered at 865 nm and 681.25 nm respectively, whilst the MGCC was calculated as

$$MGCC = \frac{R_{band\ 5}}{R_{band\ 2} + R_{band\ 5} + R_{band\ 8}} \quad (3)$$

where $R_{band\ 2}$ and $R_{band\ 5}$ are reflectance values in MERIS bands 2 and 5, centered at 442.5 nm and 560 nm respectively. Once calculated, the outlier removal procedure described in Section 2.2 was again adopted to eliminate residual noise.

2.4. Analysis of paired data

MERIS acquisitions were paired to the GCC value representing the 3 day time period within which they fell. To enable the agreement of the two data sets to be assessed, time-series of the GCC and each satellite-derived vegetation product were plotted for each study site. As the data from most study sites demonstrated a strong two-phase seasonal pattern, measures of linear correlation were ill-suited to characterising these relationships. We therefore adopted the non-parametric Spearman's rank correlation coefficient, providing a means to quantify the strength of monotonic relationships between the two variables. To investigate seasonal variations in these relationships, analysis was also carried out on spring, summer, autumn and winter subsets, which were defined according to meteorological definitions for the northern hemisphere.

2.5. Land cover data

To support interpretation of the results, high spatial resolution (30 m) land cover data were obtained from the 2011 National Land Cover Database (NLCD 2011), which consists of 20 land cover classes covering 8 broad categories (Homer et al., 2015) (Table 2). To enable the effects of land cover heterogeneity and the influence of different land cover mixtures to be assessed, the percentage of each land cover class was calculated for a 31 × 31 (930 m × 930 m) window centred on the location of each study site.

2.6. Radiative transfer modelling

To explore factors that could be responsible for the previously observed summer decline, several experiments were carried out using the Leaf Optical Properties Spectra (PROSPECT) and Scattering by Arbitrarily Inclined Leaved (SAIL) radiative transfer models (Feret et al., 2008; Jacquemoud and Baret 1990; Jacquemoud et al., 2009; Verhoef, 1984, 2007). Coupled, these models provide a physically-based means of investigating how the combined interaction of various biophysical and non-canopy variables might influence the GCC, and are particularly useful given the absence of appropriate and contemporaneous ancillary data. To this end, we extended the analysis of Wingate et al. (2015), who simulated GCC values over the course of a year, making use of input parameters that reflect empirical observations at the oak-dominated Alice Holt Research Forest in Southern England (Appendix A). The site is representative of temperate deciduous forest, having similar characteristics to many of the deciduous forest sites investigated in this study. To investigate whether variations in illumination geometry could contribute to the summer decline, we simulated the GCC using both a fixed solar zenith angle (SZA) of 30°, and a varying SZA calculated at noon for each day of year (DOY) (Fig. 2). We also carried out simulations using an alternative parameterisation of brown pigment concentration (Fig. 3), as although Wingate et al. (2015) note that the GCC is sensitive to this variable, their parameterisation poorly reflects seasonal variations typically observed in oak, with increases beginning to occur only at DOY 275. In contrast, previous research has demonstrated that increases in the concentration of brown pigments such as tannins instead begin to occur as early as DOY 150 (Feeny and Bostock, 1968).

Table 2
Classification system adopted by the NLCD 2011 (Homer et al., 2015).

Category	Classes
Water	Open water
	Perennial ice/snow
Developed	Developed (open space)
	Developed (low intensity)
	Developed (medium intensity)
	Developed (high intensity)
Barren	Barren land (rock/sand/clay)
Forest	Deciduous forest
	Evergreen forest
	Mixed forest
Shrubland	Dwarf scrub
	Shrub/scrub
Herbaceous	Grassland/herbaceous
	Sedge/herbaceous
	Lichens
	Moss
Planted/cultivated	Pasture/hay
	Cultivated crops
Wetlands	Woody wetlands
	Emergent herbaceous wetlands

3. Results

3.1. Seasonal patterns in the GCC and vegetation products derived from MERIS

Clear seasonal patterns were observed in the GCC at the majority of study sites investigated. They were best resolved at deciduous forest sites, in which the start of the growing season occurred between April and May and the end of the growing season occurred between October and November, depending on the study site. These seasonal patterns were broadly consistent with those observed in the vegetation products derived from MERIS, with the exception of the MGCC, which was subject to a substantial degree of noise (Fig. 4). At evergreen forest sites such as Howland Experimental Forest, and Wind River, the GCC was subject to a greater degree of noise (Fig. 5). Despite this, seasonal patterns were more clearly resolved by GCC than by the vegetation products derived from MERIS. Similar results were also observed at Vaira Ranch, a grassland site.

Although similar temporal patterns were observed between vegetation products derived from MERIS and GCC, they were subject to substantial differences in timing. At the start of the growing season, increases in the GCC occurred by up to 1 month prior to those in the

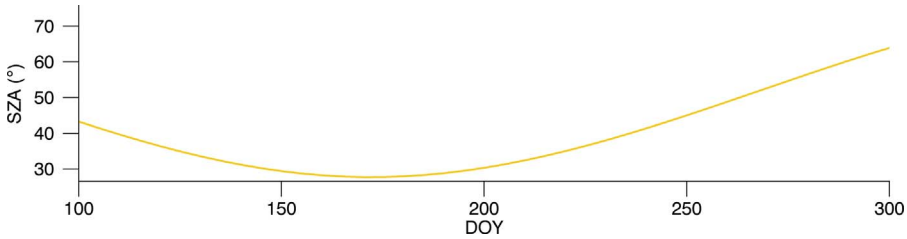

Fig. 2. Noon SZA at Alice Holt Research Forest for each DOY simulated.

vegetation products derived from MERIS. Conversely, at the end of the growing season, decreases in the vegetation products derived from MERIS occurred by up to 1 month earlier to those in the GCC. Thus, the length of the growing season observed in the vegetation products derived from MERIS was substantially shorter than in the GCC. These differences in timing were most pronounced in the case of the MGVI and MTCI (Fig. 4). Additionally, at the majority of deciduous forest sites, an asymmetric pattern was observed, in which peak GCC values occurred in late spring, before an intermediate state of more gradual decline throughout the summer (Fig. 4). This pattern was observed on an annual basis, but was not evident in the vegetation products derived from MERIS, in which peak values occurred later in the growing season.

3.2. Relationships between the GCC and vegetation products derived from MERIS

A substantial degree of variability was observed in the strength of the relationships between the GCC and each vegetation product derived from MERIS (Table 3). Moderate relationships were demonstrated by the MGVI, MTCI, and NDVI. In contrast, comparatively weak relationships were demonstrated by the MGCC. The relationships between the GCC and vegetation products derived from MERIS were also subject to a substantial degree of variability between study sites (Table 3). Moderate to strong relationships were demonstrated at study sites dominated by deciduous forest, with the exception of Hubbard Brook Experimental Forest, at which weaker relationships were demonstrated. At some study sites in which several juxtaposing land cover types dominated, such as Cary Institute of Ecosystem Studies, weaker relationships were too observed. However, this was not the case at others, such as Harvard Forest, Harvard Forest Hemlock, and Little Prospect Hill. Particularly weak relationships were demonstrated at study sites dominated by evergreen forest, such as Howland Experimental Forest and Wind River. Similarly weak relationships were observed at the grassland Vaira Ranch. In terms of seasonal differences, significant relationships between the GCC and vegetation products derived from MERIS were observed at 10 study sites during spring and 13 study sites during autumn. In contrast, significant relationships were observed at only 1 study site during the summer and 2 study sites during the winter (Appendix B).

3.3. Characteristics of the GCC

Although the range of the vegetation products derived from MERIS was relatively consistent between study sites, a greater degree of variability was observed in the range of GCC values. Additionally, the relationships between the GCC and vegetation products derived from MERIS demonstrated distinct non-linearity at some study sites, taking an exponential form (Fig. 6). The GCC was observed to saturate asymptotically at medium to high MGCC, MGVI, MTCI, and NDVI values, whilst demonstrating increased sensitivity to low levels of canopy greenness when compared to these satellite-derived vegetation products. These saturation effects were most pronounced at Morgan Monroe State Forest and Little Prospect Hill.

3.4. Factors responsible for the summer decline

The GCC values simulated using input parameters reflecting empirical observations at Alice Holt Research Forest were broadly consistent with those observed at other deciduous forest sites, taking on a similar range and seasonal pattern (Fig. 7). These simulated values were characterised by an evident spring peak, although a clear summer decline was not observed when a fixed SZA was adopted (Fig. 7). A distinct decline was observed throughout the summer months when a varying SZA was adopted as in Wingate et al. (2015), although this decline was of a relatively small magnitude compared to that observed at other deciduous forest sites investigated in this study (Fig. 7). When run with our alternative parameterisation of brown pigment concentration, the magnitude of the decline in simulated GCC values was greatly increased, better reflecting observations over these deciduous forest sites (Fig. 8).

4. Discussion

4.1. Differences in seasonal patterns observed in the GCC and satellite-derived vegetation products

The temporal inconsistencies observed between the GCC and vegetation products derived from MERIS at the start of the growing season are consistent with the results of previous studies. Similar results have been reported when the GCC has been compared with estimates of gross primary productivity (GPP) derived from eddy covariance data, in addition to a range of biophysical variables observed at both the leaf and canopy scale (Keenan et al., 2014; Toomey et al., 2015; Yang et al., 2014). It is suggested by Keenan et al. (2014) that due to the oblique angle at which the digital cameras are mounted, the effective LAI incorporated within their FOV is greater than that observed from a near-nadir viewing geometry, from which only the tops of trees are visible. Changes in canopy greenness are therefore accentuated at the start of the growing season, leading to a more rapid increase in the GCC. In addition to differences in viewing geometry, temporal inconsistencies are also to be expected because of differences in the incorporated spectral bands, which provide sensitivity to different biophysical variables. These biophysical variables have independent but related seasonal trajectories (Yang et al., 2014).

The spring peak and summer decline observed at deciduous forest sites (Fig. 4) have both been noted in previous work (Keenan et al., 2014; Toomey et al., 2015; Yang et al., 2014), and a number of explanations have been

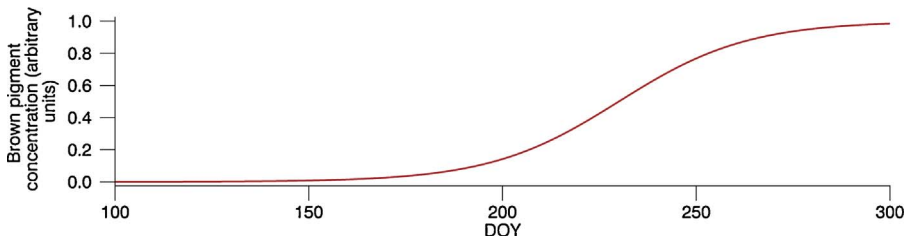

Fig. 3. Alternative brown pigment concentration parameterisation adopted to better reflect seasonal variations typically observed in oak, after Feeny and Bostock (1968).

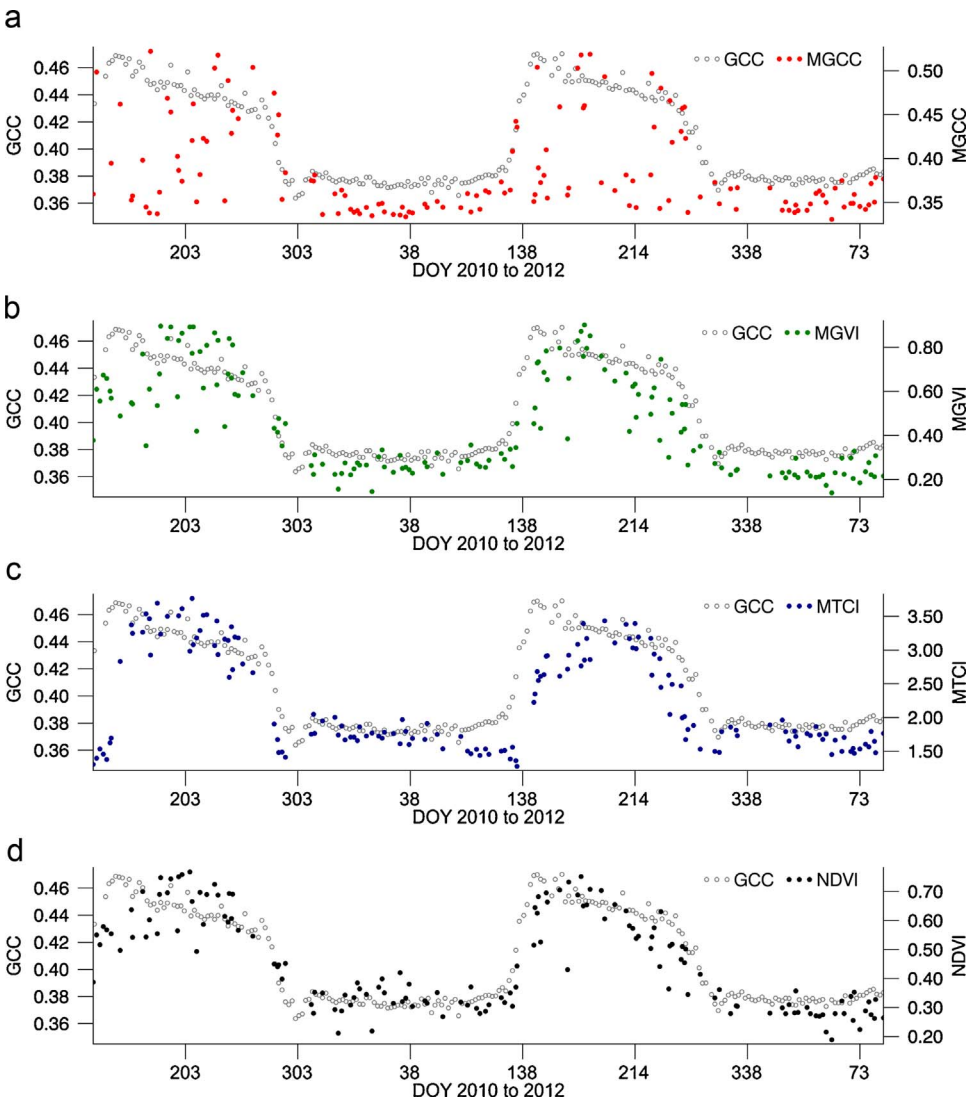

Fig. 4. Seasonal patterns in the GCC and MGCC (a), MGVI (b), MTCI (c), and NDVI (d) at Harvard Forest, a deciduous forest site.

proposed in the literature. For example, using a series of radiative transfer model experiments, Wingate et al. (2015) attributed the spring peak to the non-linear relationship between leaf chlorophyll concentration and the GCC. In early spring, increases in leaf chlorophyll concentration are initially met with increases in the GCC. Peak GCC values are reached at a leaf chlorophyll concentration of approximately 30 μg cm^{-2} during late spring, and with further increases in leaf chlorophyll concentration, a reduction in the GCC is observed. We suggest the reason for this reduction is the broadening of the chlorophyll absorption feature, which acts to reduce reflectance at green wavelengths (Gates et al., 1965; Lichtenthaler et al., 1998; Richardson et al., 2002). In terms of the summer decline, several authors have pointed to the role of leaf ageing and associated changes in pigmentation (Keenan et al., 2014; Sonnentag et al., 2012). Despite this, previous work has demonstrated that at deciduous forest sites, leaf chlorophyll concentration remains relatively constant throughout the growing season, and pronounced asymmetry is rarely observed (Gond et al., 1999; Demarez et al., 1999; Koike, 1990; Yang et al., 2014). The results of our radiative transfer modelling suggest that seasonal variations in brown pigment concentration are the major contributor to the summer decline, whilst other factors, such as seasonal variations in illumination geometry, also play a minor role.

4.2. Differences in relationships between the GCC and satellite-derived vegetation products

The moderate to strong relationships demonstrated between the GCC and MGVI, MTCI, and NDVI at deciduous forest sites reflect the results of previous studies. For example, moderate to strong relationships between the GCC and estimates of GPP derived from eddy covariance data (r^2 = 0.50–0.82) are presented by Toomey et al. (2015). At evergreen forest sites, weaker relationships are demonstrated as a result of the comparatively subtle seasonality of these species, which was poorly resolved by vegetation products derived from MERIS. It is likely that this relatively weak signal is masked by atmospheric, BRDF, and shadowing effects in the satellite-derived vegetation products, leading to substantial variability within the growing season that is unrelated to vegetation dynamics. Because these effects are less pronounced in the near-surface remote sensing data, this weak signal can be more easily resolved by the GCC. This result indicates that if MERIS and future OLCI data are to prove useful in monitoring evergreen forest sites, more rigorous atmospheric and BRDF correction schemes will be required. The weak relationships demonstrated at Vaira Ranch differ from those presented in previous studies, in which clear seasonal patterns are observed (Liu et al., 2017). In previous work over grassland sites, strong relationships between the GCC and vegetation indices derived from in-situ spectroradiometric observations have been reported (r^2 = 0.69–0.82), as have strong relationships between the GCC and estimates of GPP derived from eddy covariance data (r^2 = 0.55–0.92) (Migliavacca et al., 2011; Toomey et al., 2015). This result should therefore be treated with caution, particularly in light of the fact that only a single grassland site was investigated.

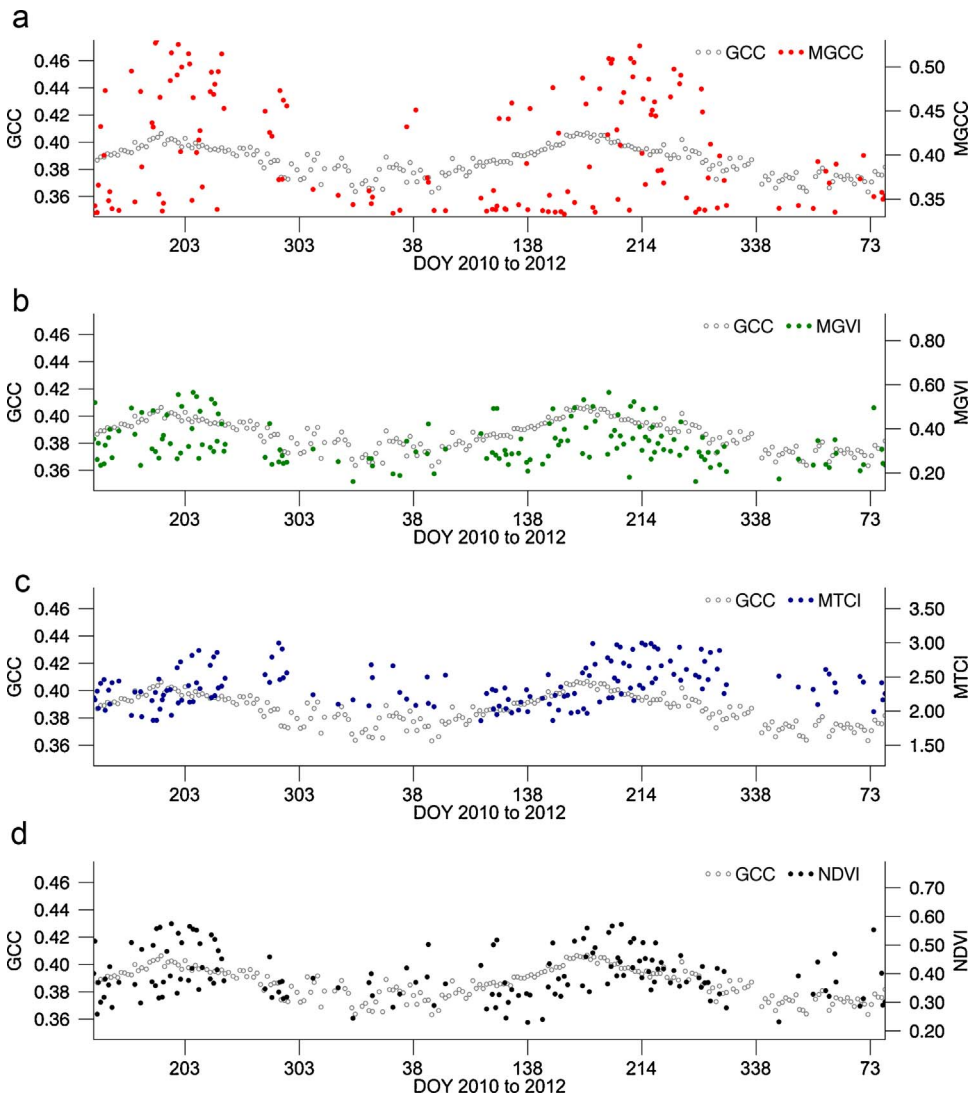

Fig. 5. Seasonal patterns in the GCC and MGCC (a), MGVI (b), MTCI (c), and NDVI (d) at Wind River, an evergreen forest site.

When comparing phenological transition dates derived from PhenoCam data and vegetation products derived from MODIS, Klosterman et al. (2014) report a strong relationship between fractional forest cover and bias in the end of spring date ($r^2 = 0.73$). Nevertheless, significant relationships ($p < 0.05$) were not reported for any other investigated phenological transition dates. Similarly, in this study, observed patterns between land cover heterogeneity and the strength of the relationships between the GCC and vegetation products derived from MERIS were varied. Weak relationships were demonstrated at some study sites dominated by several juxtaposing land cover types such as Cary Institute of Ecosystem Studies, although this was not universally the case. Others were characterised by strong relationships, reflecting the mixed nature of the findings of Klosterman et al. (2014). The observed seasonal differences in the strength and significance of these relationships are to be expected, as the degree of variation that can be explained by the GCC is substantially reduced in the summer and winter, during which the condition of vegetation remains relatively static.

An unexpected result of this study was the fact that weak relationships were demonstrated between the GCC and MGCC, as the MGCC was calculated to provide a more direct spectral comparison to the near-surface remote sensing data itself. Nevertheless, similar results were obtained by Klosterman et al. (2014), who report that when calculated from MODIS data, the GCC is subject to a substantial degree of noise, poorly representing seasonal patterns when compared to other vegetation products such as the Enhanced Vegetation Index (EVI) and NDVI. The noise observed in the MGCC is likely due to the fact that unlike the other vegetation products derived from MERIS, it incorporates a band at blue wavelengths (band 2, centered at 442.5 nm). In the optical domain, it is these shorter wavelengths that are most strongly influenced by atmospheric effects, a fact reflected by the greater degree of variation observed at all study sites in band 2 when compared to band 13 (centered at 865 nm) (Fig. 9). Because the MERIS L2 FRS data are subject only to partial atmospheric correction, residual contamination of the blue band is more likely.

4.3. Potential of near-surface remote sensing for evaluating satellite-derived vegetation products

As discussed in Section 1, near-surface remote sensing has been adopted by the phenological research community as an alternative to in-situ observations of events such as bud-burst and leaf opening. It is a particularly promising technique for the evaluation of satellite-derived phenological transition dates, enabling the phenological characteristics of an entire canopy to be characterised as opposed to those of a single plant (Hufkens et al., 2012; Keenan et al., 2014; Klosterman et al., 2014). Additionally, as the same algorithms used to derive phenological transition dates from satellite-derived vegetation products can be applied to near-surface remote sensing data, their results can be more easily compared. Consistent with the results of previous studies, clear seasonal patterns in the GCC were observed at deciduous forest sites from which it would be straightforward to derive phenological transition dates. In light of the noise observed at evergreen forest and grassland sites, another foreseeable application of near-surface

Table 3
Spearman's rank correlation coefficient (r_s) values associated with each satellite-derived vegetation product at each study site.

Study site	Land cover classes (%)	MGCC	MGVI	MTCI	NDVI
Arbutus Lake	Deciduous forest (79.9) Open water (7.8) Evergreen forest (6.3) Mixed forest (4.1) Developed open (1.9)	0.59*	0.70*	0.55*	0.72*
Bartlett Experimental Forest (IR)	Deciduous forest (59.0) Mixed forest (36.4) Shrub/scrub (2.0) Developed open (1.7)	0.33*	0.78*	0.58*	0.41*
Cary Institute of Ecosystem Studies	Deciduous forest (44.3) Pasture/hay (16.4) Evergreen forest (14.8) Developed open (9.5) Shrub/scrub (4.7) Developed low (3.6) Mixed forest (3.6) Woody wetlands (2.7)	0.35*	0.53*	0.58*	0.44*
Coweeta Hydrologic Laboratory	Deciduous forest (80.6) Developed open (12.5) Pasture/hay (2.7) Evergreen forest (1.7) Shrub/scrub (1.7)	0.39*	0.75*	0.80*	0.76*
Harvard Forest	Deciduous forest (46.2) Evergreen forest (18.7) Woody wetlands (14.9) Mixed forest (14.2) Developed open (4.4) Shrub/scrub (1.7)	0.58*	0.78*	0.64*	0.77*
Harvard Forest Hemlock	Deciduous forest (45.5) Evergreen forest (26.5) Woody wetlands (24.9) Mixed forest (2.6)	0.55*	0.76*	0.63*	0.73*
Little Prospect Hill	Deciduous forest (43.8) Mixed forest (25.2) Evergreen forest (18.1) Developed open (7.5) Woody wetlands (5.4)	0.65*	0.86*	0.76*	0.85*
Howland Experimental Forest	Evergreen forest (90.8) Woody wetlands (5.1) Mixed forest (4.0)	0.42*	0.54*	0.35*	0.50*
Hubbard Brook Experimental Forest	Deciduous forest (54.8) Mixed forest (31.7) Evergreen forest (6.7) Developed open (3.3) Cultivated crops (2.0)	0.40*	0.57*	0.48*	0.35*
Morgan Monroe State Forest	Deciduous forest (92.4) Shrub/scrub (7.6)	0.53*	0.70*	0.71*	0.59*
Proctor Maple Research Center	Deciduous forest (95.8) Evergreen forest (1.8) Woody wetlands (2.4)	0.67*	0.73*	0.62*	0.79*
University of Michigan Biological Station	Deciduous forest (85.38) Mixed forest (5.2) Grassland/herbaceous (4.3) Developed open (2.0) Evergreen forest (1.4)	0.40*	0.70*	0.81*	0.78*
Vaira Ranch	Grassland/herbaceous (79.0) Deciduous forest (11.7) Developed open (6.7) Shrub/scrub (2.6)	−0.56*	−0.71*	0.48*	−0.71*
Wind River Experimental Forest	Evergreen forest (89.2) Woody wetlands (6.0) Developed low (3.1) Shrub/scrub (1.4)	0.26*	0.50*	−0.08	0.41*

Values marked with * indicate that the relationship with the GCC was statistically significant ($p < 0.01$). For clarity, only land cover classes accounting for >1% are shown.

remote sensing data is the evaluation of cloud-screening algorithms. By analysing the DN values of an ROI covering the sky, it might be possible to automatically determine the presence or absence of cloud cover. This could provide particularly useful information in the case of instruments such as MERIS and OLCI, whose cloud-screening algorithms are constrained by the absence of bands at shortwave- and thermal-infrared wavelengths.

Despite the advantages of the technique, the results of this study reveal several issues associated with near-surface remote sensing that limit its potential for evaluation of the vegetation products that underlie satellite-derived phenological transition dates. Our analysis indicates that the relationship between the GCC and vegetation products derived from MERIS is in some cases distinctly non-linear, saturating asymptotically at medium to high MGCC, MGVI, MTCI, and NDVI values. This is an important consideration for those attempting to model variables related to plant function such as GPP,

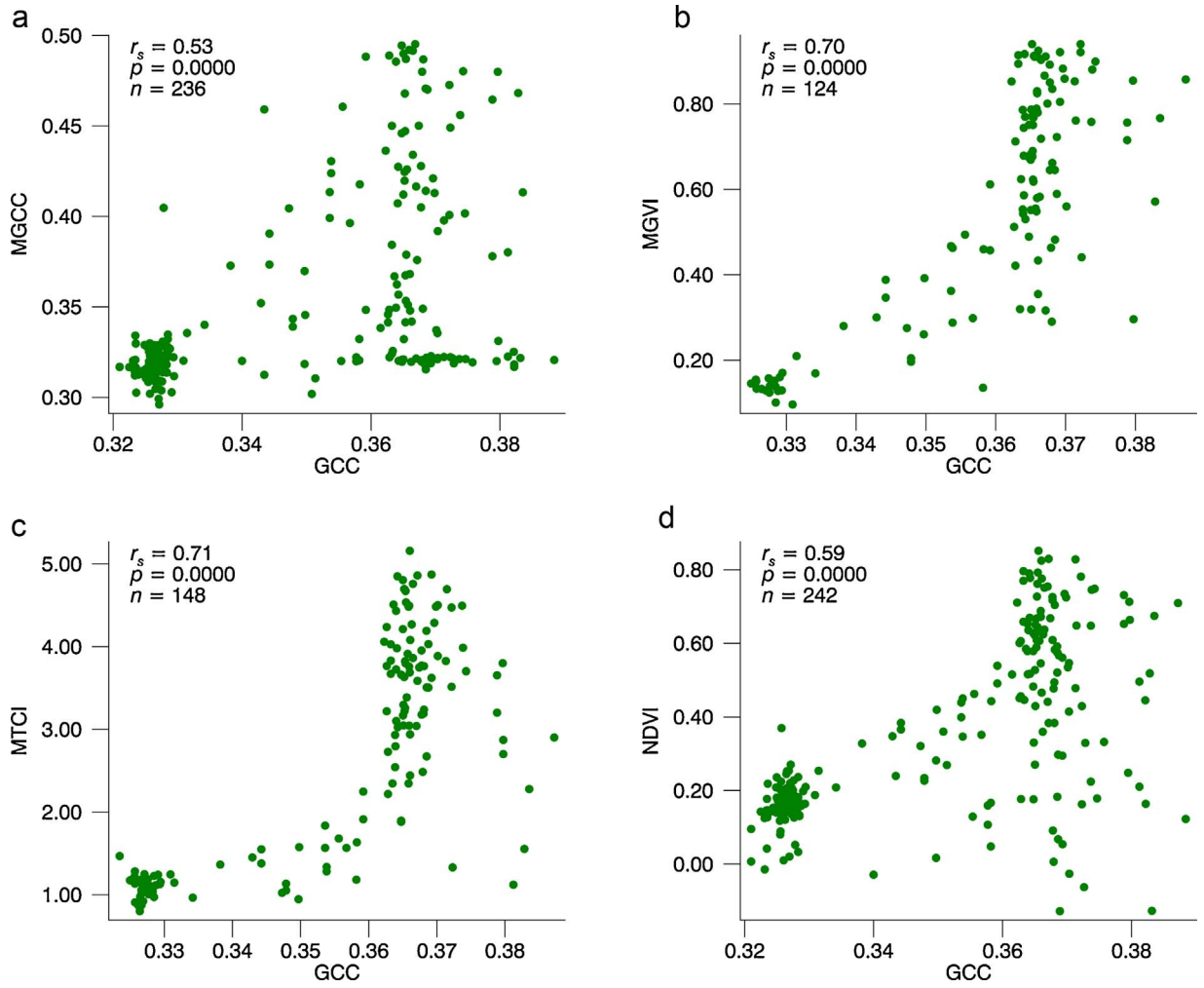

Fig. 6. Relationships between the GCC and MGCC (a), MGVI (b), MTCI (c), and NDVI (d) at Morgan Monroe State Forest, where r_s is the Spearman's rank correlation coefficient, p is the two-tailed p-value and n is the number of data points.

particularly in the case of study sites characterised by medium to high biomass. Keenan et al. (2014) note a similar non-linear relationship between the GCC and in-situ observations of LAI, suggesting that increases in the GCC occur as a result of green leaves filling gaps within the canopy. Above an LAI of approximately 2.5, few gaps remain in the canopy, and because additional leaves overlap one another, the greenness of the canopy, as observed by the digital camera, does not increase (Keenan et al., 2014). We note that the majority of satellite-derived vegetation products remain sensitive to increases in LAI, as a result of a) their near-nadir viewing geometry, and b) the fact that they incorporate bands at near-infrared wavelengths, where the reflectance of leaves is governed more strongly by structural characteristics as opposed to pigmentation. As such, the exploitation of near-infrared capabilities, as demonstrated by Petach et al. (2014) and now available at 262 PhenoCam sites, would likely enable the issue of asymptotic saturation to be at least partially overcome in future investigations.

5. Conclusions

Although near-surface remote sensing has been used to evaluate satellite-derived phenological transition dates, few studies have considered the shape and magnitude of the underlying time-series. In this study, we investigated the relationship between continuous measures of canopy greenness derived using near-surface remote sensing and satellite-derived vegetation products. Temporal inconsistencies were observed between the GCC and vegetation products derived from MERIS, reflecting the results of previous work. Although temporal inconsistencies have previously been attributed to the oblique viewing geometry of the digital cameras, they are also to be expected due to differences in the incorporated spectral bands, which provide sensitivity to different biophysical variables. As in other studies, a spring peak and summer decline were observed in the GCC at deciduous forest sites. Whilst the spring peak has previously been attributed to the non-linear relationship

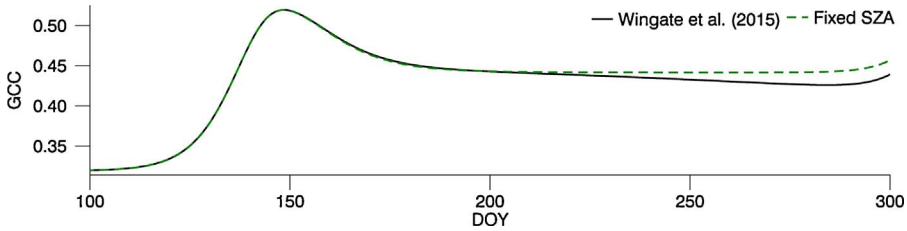

Fig. 7. GCC values simulated using a fixed SZA of 30°, in addition to a varying SZA as in Wingate et al. (2015).

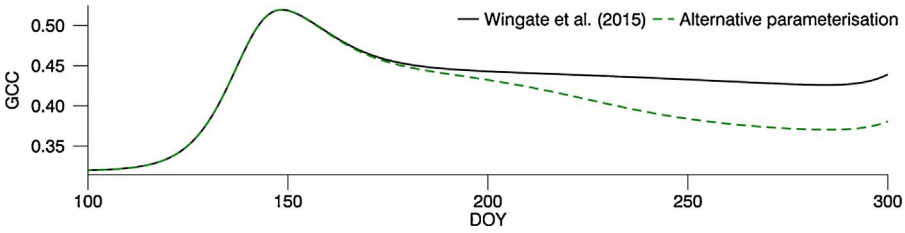

Fig. 8. GCC values simulated using the brown pigment concentation parameterisation based on that of Wingate et al. (2015), in addition to those simulated using our alternative parameterisation (Fig. 3).

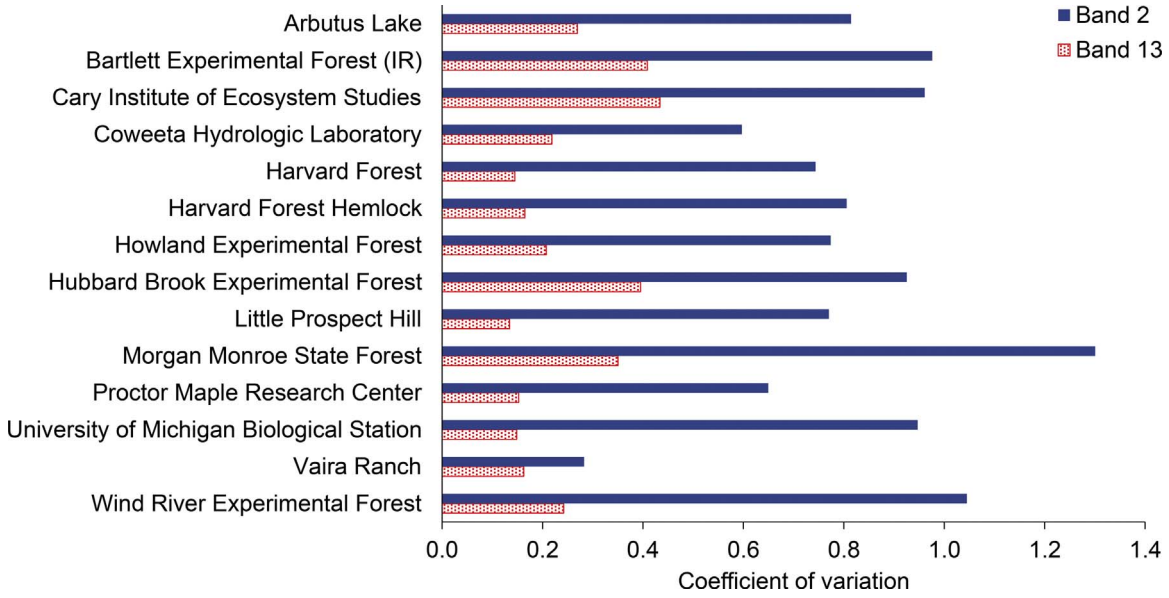

Fig. 9. Coefficient of variation associated with reflectance values in MERIS bands 2 and 13 (centered at 442.5 nm and 865 nm respectively) at each study site during the summer.

between leaf chlorophyll concentration and the GCC, the results of our radiative transfer modelling suggest that seasonal variations in brown pigment concentration, and to a lesser extent illumination geometry, contribute to the summer decline.

Moderate to strong relationships between the GCC and vegetation products derived from MERIS were demonstrated at deciduous forest sites. Weak relationships were demonstrated at evergreen forest sites as a result of their comparatively subtle seasonality, which is likely masked by atmospheric, BRDF, and shadowing effects in the vegetation products derived from MERIS. At these sites, seasonal patterns were better resolved by the GCC, highlighting the need for more rigorous atmospheric and BRDF correction schemes.

As a result of its increased sensitivity to initial increases in canopy greenness when compared to the vegetation products derived from MERIS, the GCC is particularly well-suited to identifying the start of season, making near-surface remote sensing a valuable source of data for evaluating satellite-derived phenological transition dates. Despite this, the results of this study reveal that in some cases, the relationship between the GCC and vegetation products derived from MERIS saturates asymptotically at medium to high MGCC, MGVI, MTCI, and NDVI values. At present, this limits the potential of the approach for evaluation of the vegetation products that underlie satellite-derived phenological transition dates, and for the continuous monitoring of vegetation during the growing season, particularly at medium to high biomass study sites. Nevertheless, if coupled with near-infrared capabilities, we suggest that near-surface remote sensing has the potential to serve as a useful tool for the operational and systematic evaluation of satellite-derived vegetation products.

Acknowledgements

This work was supported by ESA and a University of Southampton Vice-Chancellor's Scholarship. The authors thank the PhenoCam network for access to near-surface remote sensing data, Alessandro Burini and the G-POD team for their assistance in MERIS data processing, and Jérôme Ogée for providing the IDL routines used by Wingate et al. (2015) to simulate GCC values at Alice Holt Research Forest.

The development of PhenoCam has been supported by the Northeastern States Research Cooperative, NSF's Macrosystems Biology program (award EF-1065029), DOE's Regional and Global Climate Modelling program (award DE-SC0016011), and the US National Park Service Inventory and Monitoring Program and the USA National Phenology Network (grant number G10AP00129 from the United States Geological Survey). We acknowledge additional support, through the National Science Foundation's LTER program, for research at Harvard Forest (DEB-1237491), and Bartlett Experimental Forest (DEB-1114804).

Appendix A

See Fig. A1, Tables A1, A2

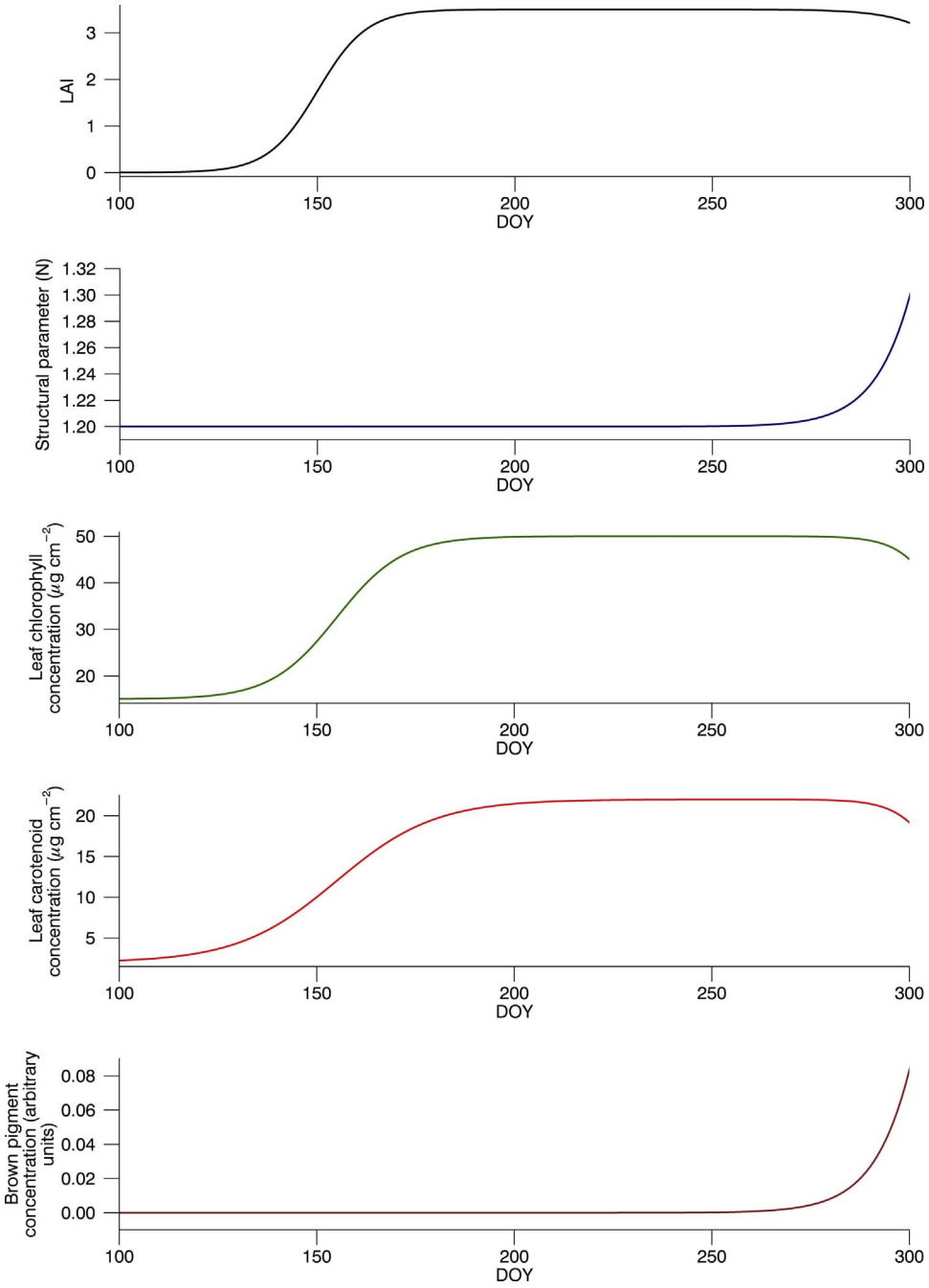

Fig. A1. Varying PROSPECT and SAIL parameters used to simulate GCC values over the course of the spring and summer at Alice Holt Research Forest, after Wingate et al. (2015). Brown pigment concentration values were rescaled to the range 0–1 for compatibility with the version of PROSPECT used in this study.

Table A1
Constant PROSPECT and SAIL parameters used to simulate GCC values over the course of the spring and summer at Alice Holt Research Forest, after Wingate et al. (2015).

Parameter	Value
Hot spot parameter	0.05
Average leaf angle (°)	30
Observer zenith angle (°)	80
Relative azimuth angle (°)	0
Diffuse to direct radiation (%)	25
Soil coefficient	0.2
Water thickness (cm)	0.04
Dry matter (g cm^{-2})	0.008

Table A2
Details of the wavelengths averaged to approximate the red, green and blue bands of a digital camera from PROSPECT and SAIL output spectra.

Band	Wavelength (nm)		
	Minimum	Centre	Maximum
Blue	400	450	500
Green	500	550	600
Red	600	650	700

Appendix B

See Table B1

Table B1
Spearman's rank correlation coefficient (r_s) values associated with each satellite-derived vegetation product at each study site, by season. Values marked with * indicate that the relationship with the GCC was statistically significant ($p < 0.01$).

Site	Spearman's rank correlation coefficient															
	Spring				Summer				Autumn				Winter			
	MGCC	MGVI	MTCI	NDVI	MGCC	MGVI	MTCI	NDVI	MGCC	MGVI	MTCI	NDVI	MGCC	MGVI	MTCI	NDVI
Arbutus Lake	0.66*	0.44	−0.47	0.56	0.07	0.48	0.61	0.25	0.49	0.59*	0.63*	0.69*	0.37	0.01	−0.12	−0.11
Bartlett Experimental Forest (IR)	0.29	0.50*	−0.04	0.28	−0.21	0.22	0.07	−0.07	0.25	0.87*	0.66*	0.26	0.22	0.14	0.01	0.07
Cary Institute of Ecosystem Studies	0.47*	0.81*	0.70*	0.67*	0.22	0.01	0.06	0.06	0.25	0.51	0.57*	0.24	−0.12	−0.17	0.46	0.09
Coweeta Hydrologic Laboratory	0.33	0.77*	0.73*	0.81*	−0.11	0.28	0.27	0.29	0.25	0.68*	0.91*	0.77*	0.23	0.42	−0.03	0.18
Harvard Forest	0.62*	0.61*	0.23	0.58*	−0.01	0.00	−0.32	0.09	0.49*	0.71*	0.80*	0.74*	0.16	−0.30	−0.06	−0.33
Harvard Forest Hemlock	0.44	0.33	0.23	0.27	−0.11	0.07	−0.23	0.08	0.30	0.65*	0.66*	0.68*	0.11	−0.15	0.03	−0.12
Little Prospect Hill	0.47	0.64*	0.03	0.61	0.19	0.24	−0.04	0.25	0.52*	0.80*	0.87*	0.83*	−0.23	0.16	0.10	0.20
Howland Experimental Forest	0.67*	0.33	−0.38	0.26	0.14	0.05	−0.34	0.07	0.16	0.59*	0.35	0.55*	0.51*	0.18	−0.16	0.25
Hubbard Brook Experimental Forest	0.33	0.49	−0.16	0.06	0.14	−0.11	−0.05	0.24	0.43	0.34	0.22	0.19	0.13	−0.25	−0.09	−0.08
Morgan Monroe State Forest	0.42*	0.76*	0.49*	0.48*	−0.04	0.15	0.11	−0.16	0.44*	0.72*	0.88*	0.52*	0.29	0.00	0.63*	−0.03
Proctor Maple Research Center	0.63*	0.87*	0.41	0.84*	−0.20	−0.14	−0.35	−0.08	0.57*	0.73*	0.79*	0.83*	−0.05	0.22	−0.25	0.30
University of Michigan Biological Station	0.66	0.90*	−0.24	0.90*	0.01	0.04	0.45	0.22	0.64	0.85*	0.81*	0.93*	–	–	–	–
Vaira Ranch	0.04	0.38	0.04	0.23	−0.39*	−0.57*	0.23*	−0.60*	−0.65*	−0.84*	0.71*	−0.86*	0.43	−0.49	−0.07	−0.34
Wind River Experimental Forest	−0.01	0.00	−0.09	−0.13	−0.21	−0.05	−0.23	−0.04	0.04	0.48*	0.12	0.50	−0.12	0.11	−0.17	0.07

References

Baret, F., Weiss, M., Allard, D., Garrigue, S., Leroy, M., Jeanjean, H., Fernandes, R., Myneni, R., Privette, J., Morisette, J., Bohbot, H., Bosseno, R., Dedieu, G., Di Bella, C., Duchemin, B., Espana, M., Gond, V., Gu, X.F., Guyson, D., Lelong, C., Maisongrande, P., Mougin, E., Nilson, T., Verousraete, F., Vintilla, R., 2005. VALERI: a Network of Sites and a Methodology for the Validation of Medium Spatial Resolution Land Satellite Products. IRNA, Avignon, France.

Baret, F., Hagolle, O., Geiger, B., Bicheron, P., Miras, B., Huc, M., Berthelot, B., Niño, F., Weiss, M., Samain, O., Roujean, J.L., Leroy, M., 2007. LAI, fAPAR and fCover CYCLOPES global products derived from VEGETATION: part 1: principles of the algorithm. Remote Sens. Environ. 110 (3), 275–286.

Barker, K., Mazeran, C., Lerebourg, C., Bouvet, M., Antoine, D., Ondrusek, M., Zibordi, G., Lavender, S., 2008. MERMAID: the MERIS matchup in-situ database. In: Proceedings of the 2nd MERIS/(A)ATSR User Workshop, September 2008. Frascati, Italy.

Barnes, W.L., Pagano, T.S., Salomonson, V.V., 1998. Prelaunch characteristics of the moderate resolution imaging spectroradiometer (MODIS) on EOS-AM1. IEEE Trans. Geosci. Remote Sens. 36 (4), 1088–1100.

Baumann, M., Ozdogan, M., Richardson, A.D., Radeloff, V.C., 2017. Phenology from Landsat when data is scarce: using MODIS and dynamic time-warping to combine multi-year Landsat imagery to derive annual phenology curves. Int. J. Appl. Earth Obs. Geoinf. 54, 72–83.

Carlson, T.N., Ripley, D.A., 1997. On the relation between NDVI, fractional vegetation cover, and leaf area index. Remote Sens. Environ. 62 (3), 241–252.

Coops, N.C., Hilker, T., Bater, C.W., Wulder, M.A., Nielsen, S.E., McDermid, G., Stenhouse, G., 2012.. Linking ground-based to satellite-derived phenological metrics in support of habitat assessment. Remote Sens. Lett. 3 (3), 192–200.

Dash, J., Curran, P.J., 2004. The MERIS terrestrial chlorophyll index. Int. J. Remote Sens. 25 (23), 5403–5413.

Demarez, V., Gastellu-Etchegorry, J.P., Mougin, E., Marty, G., Proisy, C., Dufrêne, E., le Dantec, V., 1999. Seasonal variation of leaf chlorophyll content of a temperate forest: inversion of the PROSPECT model. Int. J. Remote Sens. 20 (5), 879–894.

Donlon, C., Berruti, B., Buogiorno, A., Ferreira, M.H., Féménias, P., Frerick, J., Goryl, P., Klein, U., Laur, H., Mavrocordatos, C., Nieke, J., Rebhan, H., Seitz, V., Stroede, J., Sciarra, R., 2012. The global monitoring for environment and security (GMES) Sentinel-3 mission. Remote Sens. Environ. 120, 37–57.

EC, 2005. Global Monitoring for Environment and Security (GMES): From Concept to Reality. European Commission, Brussels.

ESA, 2006. MERIS Products Quality Status Report: MEGS 7.4 and IPF 5. European Space Agency, Frascati Italy.

ESA, 2012. Sentinel-3. ESA's Global Land and Ocean Mission for GMES Operational Services. European Space Agency Communications, Noordwijk, Netherlands.

FAO, 2010. Global Forest Resources Assessment 2010: Main Report. Food and Agriculture Organisation of the United Nations, Rome.

Feeny, P.P., Bostock, H., 1968. Seasonal changes in the tanning content of oak leaves. Phytochemistry 7 (5), 871–880.

Féret, J.B., François, C., Asner, G.P., Gitelson, A.A., Martin, R.E., Bidel, L.P.R., Ustin, S.L., le Maire, G., Jacquemoud, S., 2008. PROSPECT-4 and 5: advances in the leaf optical properties model separating photosynthetic pigments. Remote. Sens. Environ. 120 (6), 3030–3043.

Fernandes, R., Plummer, S., Nightingale, J., Baret, F., Camacho, F., Fang, H., Garrigues, S., Gobron, N., Lang, M., Lacaze, R., LeBlanc, S., Meroni, M., Martinez, B., Nilson, T., Pinty, B., Pisek, J., Sonnentag, O., Verger, A., Welles, J., Weiss, M., Widlowski, J.L., 2014. Global leaf area index product validation good practices. In: Schaepman-Strub, G., Román, M., Nickeson, J. (Eds.), Best Practice for Satellite-Derived Land Product Validation. Committee on Earth Observation Satellites Working Group on Calibration and Validation, Greenbelt, Maryland, United States.

Foley, J.A., Ramankutty, N., Brauman, K.A., Cassidy, E.S., Gerber, J.S., Johnston, M., Mueller, N.D., O'Connell, C., Ray, D.K., West, P.C., Balzer, C., Bennet, E.M., Carpenter, S.R., Hill, J., Monfreda, C., Polasky, S., Rockström, J., Sheehan, J., Siebert, S., Tilman, D., Zaks, D.P.M., 2011. Solutions for a cultivated planet. Nature 478 (7369), 337–342.

Gómez-Chova, L., Camps-Valls, G., Calpe-Maravilla, J., Guanter, L., Moreno, J., 2007. Cloud-screening algorithms for ENVISAT/MERIS multispectral images. IEEE Trans. Geosci. Remote Sens. 45 (12), 4105–4118.

GCOS. 2012, GCOS Essential Climate Variables [online], Global Climate Observing System, available: http://www.wmo.int/pages/prog/gcos/index.php. (Accessed 19. 9.2016).

Gates, D.M., Keegan, H.J., Schleter, J.C., Weidner, V.R., 1965. Spectral properties of

plants. Appl. Opt. 4 (1), 11–20.
Gobron, N., Pinty, B., Verstraete, M., Govaerts, Y., 1999. The MERIS global vegetation index (MGVI): description and preliminary application. Int. J. Remote Sens. 20 (9), 1917–1927.
Godfray, C.H., Beddington, J.R., Crute, I.R., Haddad, L., Lawrence, D., Muir, J.F., Pretty, J., Robinson, S., Thomas, S.M., Toulmin, C., 2010. Food security: the challenge of feeding 9 billion people. Science 327 (5967), 812–818.
Gond, V., de Pury, D.G.G., Veroustraete, F., Ceulemans, R., 1999. Seasonal variations in leaf area index, leaf chlorophyll, and water content; scaling-up to estimate fAPAR and carbon balance in a multilayer, multispecies forest. Tree Physiol. 19, 673–679.
Homer, C.G., Dewitz, J.A., Yang, L., Jin, S., Danielson, P., Xian, G., Coulston, J., Herold, N.D., Wickham, J.D., Megown, K., 2015. Completion of the 2011 National Land Cover Database for the conterminous Unites States–representing a decade of land cover change information. Photogramm. Eng. Remote Sens. 81 (5), 345–354.
Hufkens, K., Friedl, M., Sonnentag, O., Braswell, B.H., Milliman, T., Richardson, A.D., 2012. Linking near-surface and satellite remote sensing measurements of deciduous broadleaf forest phenology. Remote Sens. Environ. 117, 307–321.
Ide, R., Oguma, H., 2010. Use of digital cameras for phenological observations. Ecol. Inf. 10, 1689–1706.
Jacquemoud, S., Baret, F., 1990. PROSPECT: a model of leaf optical properties spectra. Remote Sens. Environ. 34, 75–91.
Jacquemoud, S., Verhoef, W., Baret, F., Bacour, C., Zarco-Tejada, P.J., Asner, G.P., François, C., Ustin, S.L., 2009. PROSPECT + SAIL models: a review of use for vegetation characterization. Remote Sens. Environ. 113, S56–S66.
Justice, C., Belwards, A., Morisette, J., Lewis, P., Privette, J., Baret, F., 2000. Developments in the 'validation' of satellite sensor products for the study of the land surface. Int. J. Remote Sens. 21 (17), 3383–3390.
Justice, C.O., Román, M.O., Csiszar, I., Vermote, E.F., Wolfe, R.E., Hook, S.J., Friedl, M., Wang, Z., Schaaf, C.B., Mirua, T., Tschudi, M., Riggs, G., Hall, D.K., Lyapustin, A.I., Devadiga, S., Davidson, C., Masuoka, E.J., 2013. Land and cryosphere products from NPP VIIRS: overview and status. J. Geophys. Res. Atmos. 118 (17), 9753–9765.
Keenan, T.F., Darby, B., Felts, E., Sonnentag, O., Fridel, M.A., Hufkens, K., O'Keefe, J., Klosterman, S., Munger, J.W., Toomey, M., Richardson, A.D., 2014. Tracking forest phenology and season physiology using digital repeat photography: a critical assessment. Ecol. Appl. 24 (6), 1478–1489.
Klosterman, S.T., Hufkens, K., Gray, J.M., Melaas, E., Sonnentag, O., Lavine, I., Mitchell, L., Norman, R., Friedl, M.A., Richardson, A.D., 2014. Evaluating remote sensing of deciduous forest phenology at multiple spatial scales using PhenoCam imagery. Biogeosciences 11, 4305–4320.
Knyazikhin, Y., Glassy, J., Privette, J.L., Tian, Y., Lotsch, A., Zhang, Y., Wang, Y., Morisette, J.T., Votava, P., Myneni, R.B., Nemani, R.R., Running, S.W., 1999. MODIS Leaf Area Index (LAI) and Fraction of Photosynthetically Active Radiation Absorbed by Vegetation (FPAR) Product (MOD15) Algorithm Theoretical Basis Document. Boston University, Boston, United States.
Koike, T., 1990. Autumn coloring, photosynthetic performance and leaf development of deciduous broad-leaved trees in relation to forest succession. Tree Physiol. 7, 21–32.
Lichenthaler, H.K., Wenzel, O., Buschmann, C., Gitelson, A., 1998. Plant stress detection by reflectance and fluorescence. Ann. N.Y. Acad. Sci. 851, 271–285.
Liu, Y., Hill, M.J., Zhang, M., Wang, Z., Richardson, A.D., Hufkens, K., Filippa, G., Baldocchi, D.D., Ma, S., Verfaillie, J., Schaaf, C.B., 2017. Using data from Landsat, MODIS, VIIRS and PhenoCams to monitor the phenology of California oak/grass savanna and open grassland across spatial scales. Agric. For. Meterol. 237–238, 311–325.
Mélin, F., Zibordi, G., Berthon, J., Bailey, S., Franz, B., Voss, K., Flora, S., Grant, M., 2011. Assessment of MERIS reflectance data as processing with SeaDAS over the European seas. Opt. Express 19 (25), 25657–25671.
Maisongrande, P., Duchemin, B., Dedieu, G., 2004. VEGETATION/SPOT: an operational mission for the Earth monitoring; presentation of new standard products. Int. J. Remote Sens. 25 (1), 9–14.
Migliavacca, M., Galvagno, M., Cremonese, E., Rossini, M., Meroni, M., Sonnentag, O., Cogliati, S., Manc, G., Diotri, F., Busetto, L., Cescatti, A., Colombo, R., Fava, F., Morra di Cella, U., Pari, E., Siniscalco, C., Richardson, A.D., 2011. Using digital repeat photography and eddy covariance data to model grassland phenology and photosynthetic CO_2 uptake. Agric. For. Meteorol. 151 (10), 1325–1337.
Morisette, J.T., Privette, J.L., Justice, C.O., 2002. A framework for the validation of MODIS land products. Remote Sens. Environ. 83 (1), 77–96.
Morisette, J.T., Baret, F., Privette, J., Myneni, R.B., Nickeson, J.E., Garrigues, S., Shabanov, N.V., Weiss, M., Fernandes, R.A., Leblanc, S.G., Kalacska, M., Sánchez-Azofeifa, G.A., Chubey, M., Rivard, B., Stenberg, P., Rautiainen, M., Voipio, P., Manninen, T., Pilant, A.N., Lewis, T.E., Iiames, J.S., Colombo, R., Meroni, M., Busetto, L., Cohen, W.B., Turner, D.P., Warner, E.D., Petersen, G.W., Seufert, G., Cook, R., 2006. Validation of global moderate-resolution LAI products: a framework proposed within the CEOS land product validation subgroup. IEEE Trans. Geosci. Remote Sens. 44 (7), 1804–1817.
Morra di Cella, U., Bocca, M., Busetto, L., Colombo, R., Cremonese, E., Delestrade, A., Galvagno, M., Loison, A., Lopez, J.F., Meroni, M., Migliavacca, M., Tutino, S., Yoccoz, N.G., 2009. PHENOALP: a new project on phenology in the Western Alps. In: Proceedings of the 4th Symposium of the Hohe Tauren National Park for Research in Protected Areas, September 2009. Kaprun, Salzburg, Austria.
Myneni, R.B., Williams, D.L., 1994. On the relationship between FAPAR and NDVI. Remote Sens. Environ. 49 (3), 200–211.
Myneni, R.B., Hoffman, S., Knyazikhim, Y., Privette, J.L., Glassy, J., Tian, Y., Wang, Y., Song, X., Zhang, Y., Smith, G.R., Lotsch, A., Friedl, M., Morisette, J.T., Votava, P., Nemani, R.R., Running, S.W., 2002. Global products of vegetation leaf area and fraction absorbed PAR from year one of MODIS data. Remote Sens. Environ. 83 (1), 214–231.
Nijland, W., Bolton, D.K., Coops, N.C., Stenhouse, G., 2016. Imaging phenology: scaling from camera plots to landscapes. Remote Sens. Environ. 177, 13–20.
Petach, A.R., Toomey, M., Aubrecht, D.M., Richardson, A.D., 2014. Monitoring vegetation phenology using an infrared-enabled security camera. Agric. For. Meteorol. 195–196, 143–151.
QA4EO, 2010. Quality Assurance Framework for Earth Observation [online], available: http://qa4eo.org/. (Accessed 19.9.2016).
Rast, M., Bézy, J.L., Bruzzi, S., 1999. The ESA Medium Resolution Imaging Spectrometer (MERIS): a review of the instrument and its mission. Int. J. Remote Sens. 20 (9), 1681–1702.
Richardson, A.D., Duigan, S.P., Berlyn, G.P., 2002. An evaluation of noninvasive methods to estimate foliar chlorophyll content. New Phytol. 153, 185–194.
Richardson, A.D., Jenkins, J.P., Braswell, B.H., Hollinger, D.Y., Ollinger, S.V., Smith, M., 2007. Use of digital webcam images to track spring green-up in a deciduous broadleaf forest. Oecologia 152 (2), 323–334.
Richardson, A.D., Braswell, B.H., Hollinger, D.Y., Jenkins, J.P., Ollinger, S.V., 2009. Near-surface remote sensing of spatial and temporal variation in canopy phenology. Ecol. Appl. 19 (6), 1417–1428.
Rouse, J.W., Haas, R.H., Schell, J.A., Deering, D.W., 1973. Monitoring vegetation systems in the Great Plains with ERTS. Proceedings of the Third Earth Resources Technology Satellite-1 Symposium, December 1973. Goddard Space Flight Centre, Washington D.C United States.
Sá, C., D'Alimonte, D., Brito, A.C., Kajiyama, T., Mendes, C.R., Vitorino, J., Oliveira, P.B., da Silva, J.C.B., Brotas, V., 2015. Validation of standard and alternative satellite ocean-colour chlorophyll products off Western Iberia. Remote Sens. Environ. 168, 403–419.
Santer, R., Carrere, V., Dubuisson, P., Roger, J.C., 1999. Atmospheric correction over land for MERIS. Int. J. Remote Sens. 20 (9), 1819–1840.
Sellers, P.J., Dickinson, R.E., Randall, D.A., Betts, A.K., Hall, F.G., Berry, J.A., Collatz, G.J., Denning, A.S., Mooney, H.A., Nobre, C.A., Sato, N., Field, C.B., Henderson-Sellers, A., 1997. Modelling the exchanges of energy, water, and carbon between continents and the atmosphere. Science 275 (5299), 502–509.
Sonnentag, O., Hufkens, K., Teshera-Sterne, C., Young, A.M., Friedl, M., Braswell, B.H., Milliman, T., O'Keefe, J., Richardson, A.D., 2012. Digital repeat photography for phonological research in forest ecosystems. Agric. For. Meteorol. 152, 159–177.
Toomey, M., Friedl, M.A., Frolking, S., Hufkens, K., Klosterman, S., Sonnentag, O., Baldocchi, D.D., Bernacchi, C.J., Biraud, S.C., Bohrer, G., Brzostek, E., Burns, S.P., Coursolle, C., Hollinger, D.Y., Margolis, H.A., McCaughey, H., Monson, R.K., Munger, J.W., Pallardy, S., Phillips, R.P., Torn, M.S., Wharton, S., Zeri, M., Richardson, A.D., 2015. Greenness indices from digital cameras predict the timing and seasonal dynamics of canopy-scale photosynthesis. Ecol. Appl. 25 (1), 99–115.
Verhoef, W., Xiao, Q., Jia, L., Su, Z., 2007. Unified optical-thermal four-stream radiative transfer theory for homogeneous vegetation canopies. IEEE Trans. Geosci Remote Sens. 45 (6), 1808–1822.
Verhoef, W., 1984. Light scattering by leaf layers with application to canopy reflectance modelling: the SAIL model. Remote Sens. Environ. 16, 125–141.
Wingate, L., Ogée, J., Cremonese, E., Filippa, G., Mizunuma, T., Migliavacca, M., Moisy, C., Wilkinson, M., Moureaux, C., Wohlfahrt, G., Hammerle, A., Hörtnagl, L., Gimeno, C., Porcar-Castell, A., Galvagno, M., Nakaji, T., Morison, J., Kolle, O., Knohl, A., Kutsch, W., Kolari, P., Nikinmaa, E., Ibrom, A., Gielen, B., Eugster, W., Balzarolo, M., Papale, D., Klumpp, K., Köstner, B., Gründwald, T., Joffre, R., Ourcival, J.M., Hellstrom, M., Lindroth, A., Charles, G., Longdoz, B., Genty, B., Levula, J., Heinsch, B., Sprintsin, M., Yakir, D., Manise, T., Guyon, D., Ahrends, H., Plaza-Aguilar, A., Gaun, J.H., Grace, J., 2015. Interpreting canopy development and physiology using the EUROPHEN camera network at flux sites. Biogeosciences 12, 7979–8034.
Yang, X., Tang, J., Mustard, J.F., 2014. Beyond leaf colour: comparing camera-based phenological metrics with leaf biochemical, biophysical and spectral properties throughout the growing season of a temperate deciduous forest. J. Geophys. Res. Biogeosci. 119 (3), 181–191.